






# Suzuki–Miyaura reaction and solventfree oxidation of benzyl alcohol by Pd/nitrogen-doped CNTs catalyst

Ayomide H. Labulo<sup>1</sup> , Bernard Omondi<sup>1</sup> , and Vincent O. Nyamori<sup>1,\*</sup> 

<sup>1</sup> School of Chemistry and Physics, University of KwaZulu-Natal, Westville Campus, Private Bag X54001, Durban, South Africa

Received: 20 June 2018

Accepted: 25 July 2018

Published online:

2 August 2018

© Springer Science+Business Media, LLC, part of Springer Nature 2018

## ABSTRACT

Suzuki–Miyaura C–C coupling reactions were investigated with Pd/nitrogen-doped carbon nanotubes (Pd/N-CNTs) as a catalyst. Also, the same catalyst was examined for the solventfree oxidation of benzyl alcohol to benzaldehyde. Nitrogen-doped carbon nanotubes (N-CNTs) were synthesized from 1-ferrocenylmethyl(2-methylimidazole) and benzophenone via a chemical vapour deposition technique. Acetonitrile was used as a solvent and source of both carbon and nitrogen constituents of N-CNTs. Pd nanoparticles (Pd NPs) were successfully dispersed on N-CNTs via a metal organic chemical vapour deposition method. SEM, TEM, XRD, elemental analysis and ICP-OES measurements were used to characterize the nanomaterials. From the TEM analysis, it was observed that Pd NPs were spherical and with particle sizes ranging from 3 to 8 nm. For Suzuki C–C coupling reactions, phenylboronic acid, aryl halide, Pd/N-CNTs catalyst and a base (NaOAc, K<sub>2</sub>PO<sub>4</sub>, K<sub>2</sub>CO<sub>3</sub>, NaOH, Et<sub>3</sub>N and Na<sub>2</sub>CO<sub>3</sub>) were used. The optimized experiments indicate that K<sub>2</sub>CO<sub>3</sub>, as the base, and ethanol/water (1:1 v/v, 10 mL) mixture, as a solvent, are the best reaction conditions. The solventfree oxidation reactions of benzyl alcohol were also done with Pd/N-CNTs catalyst and benzyl alcohol as a substrate. In both sets of reactions, C–C coupling and oxidation, the increase in pyrrolic nitrogen species was found to be responsible for higher catalytic activities of Pd/N-CNT catalysts, and this was attributed to the ease of Pd NP dispersion on N-CNTs, relative to pristine CNTs. Also, the higher catalytic activity of Pd/N-CNTs could be ascribed not only to the smaller Pd NP size or surface area, but to also the surface properties and the nature of the support when compared with the undoped counterpart, Pd/CNTs.

## Introduction

Efficient Suzuki coupling reaction of an aryl halide and boronic acids with less expensive substrates, and recyclable heterogeneous catalysts, is of economic

importance for pharmaceutical and fine chemical industries. The selective oxidation of benzyl alcohol with the use of molecular oxygen is one of the favourable routes for a greener synthesis of benzaldehyde [1], i.e. relative to metal oxidants such as

Address correspondence to E-mail: nyamori@ukzn.ac.za

permanganates and chromates. Benzaldehyde is an important intermediate in organic synthesis due to its application in the pharmaceutical [2], cosmetic [3] and food packaging [4] industries, among other useful applications. On the other hand, palladium (Pd) metal has been intensively used as a catalyst in a wide range of catalytic processes, such as oxidation [5], hydrogenation [6, 7] and C–C coupling reactions [8, 9]. Pd metal catalyst has been found to be very useful, especially in homogeneous catalysis as it is relatively more selective, however, the use of homogenous Pd metal catalyst remains a challenge and uneconomical for large-scale preparation. Hence, heterogeneous catalysis is sometimes preferred. Under heterogeneous catalysis, Pd nanoparticles (Pd NPs) have been supported on several substrates such as zeolites [10], polymers [11] and metal oxides [12, 13] for improved catalytic activity.

Due to poor interactions between catalyst active sites and reactants, coupled with the unavailability of active site on some aforementioned supports, shaped carbon nanomaterials (SCNMs), such as carbon nanotubes (CNTs), carbon sphere (CS), carbon fibres (CF) and graphene, are among the most sought-after alternative supports. In the case of CNTs, they are known to enhance the deposition of active metal crystallites and regulate substrates access on supported metal nanoparticles [14]. Reports also show that CNTs demonstrate superior catalytic activity due to their enhanced thermal stability and larger surface area, which is tuneable when employed as catalyst support [15–17].

CNTs have been synthesized via several methods: namely, arc discharge [18], laser ablation [19] and CVD techniques [20]. Among these methods, the CVD technique is widely employed for CNTs synthesis, and this is due to their relatively high deposition rates, easy scale-up and relatively easy removal of impurities from gaseous precursors [21]. CNTs have been employed as a support for metal nanoparticles for several catalytic applications due to their unique structural and electronic properties [22, 23]. The introduction of heteroatoms such as nitrogen into the graphitic matrix to give N-CNTs improves their potential catalytic applications, due to improved bulk and surface properties [24]. Similarly, CNTs surface modification via acid treatment introduces oxygen-functionalized groups (i.e. hydroxyl, carbonyl, lactones and quinone) on the N-CNTs surface which act as additional anchoring sites (apart

from the N-heteroatom) for Pd ions where the nucleation and growth of palladium nanoparticles (Pd NPs) are enhanced. Incorporation of these atoms (i.e. oxygen and nitrogen) introduces defects in CNTs [25]. These defects modify the dispersion, morphology, electronic structure, stability and surface area and ultimately enhance the catalytic performance of supported metal nanoparticles [26].

Pd nanoparticles as a catalyst have been widely employed for C–C coupling reactions; however, one of the setbacks in Pd heterogeneous catalysis is the Pd leaching aspect [27]. Heidenreich et al. [28] reported that Pd leaching could be prevented by fine-tuning of reaction conditions such as increasing reaction temperature and the introduction of reducing agents. However, this results in an increase in palladium particle size which leads to catalyst deactivation. Nevertheless, catalytic activities of CNTs as carbon support for Pd catalysts have been reported, especially for C–C coupling [29] and benzyl alcohol oxidation reactions [30]. However, there is not much work reported on the application of Pd/N-CNTs as supports for these reactions. Methods, such as electrodeposition [31] and metal–organic chemical vapour deposition (MOCVD) [32], have been employed for the deposition of Pd NPs on N-CNTs with latter approach still being the most efficient, cost-effective and environmentally friendly method [33].

There has been a lot of interest in Pd NPs supported on CNTs, and this is an ongoing research with continuous attempts towards modifying CNTs surface chemistry in order to improve the efficiency and greenness of the catalysts [34]. Interestingly, Pd NPs supported on N-CNTs have displayed promising catalytic activities in Heck coupling reactions [35], solventfree oxidation of benzaldehyde [36], Suzuki coupling [37] and hydrogenation reactions [38–40]. This has been associated with the type of nitrogen species incorporated [35, 41]. However, one of the major setbacks of Pd NPs anchored on N-CNTs is the uneven distribution of nanoparticles [42]. Hence, there is interest in achieving uniform dispersion of Pd NPs onto N-CNTs. To achieve better dispersion, oxygen functional groups such as carbonyl, carboxyl, lactone and quinone can be introduced in situ in the reactant mixture using water [43] or oxygen-containing aromatic compounds such as ethylbenzoate and benzaldehyde [44] to enhance N-CNTs wettability, thus leading to improved catalytic activity of N-CNTs. Also, the introduced surface oxygen

functionalities can enhance the dispersion of Pd NPs by acting as the anchoring sites [27]. Duan et al. [45] reported the fabrication of Pd NPs supported on mesoporous N-CNTs with ultrafine well-dispersed Pd NPs of 2–3 nm diameter size by the impregnation method. The improved catalytic performance of the Pd/N-CNTs catalyst was attributed to a strong interaction between Pd NPs and pyridinic-N atoms incorporated into the N-CNTs [45].

Herein, we report for the first time the use of 1-ferrocenylmethyl(2-methylimidazole) as a catalyst for the synthesis of N-CNTs. Also, the effect of oxygen on the surface properties of N-CNTs during synthesis has been investigated. In this study, the effect of oxygen-treated N-CNTs on Pd NPs properties such as particle size, stability and its dispersion on the catalytic activity and selectivity, compared to CNTs and N-CNTs counterpart, was explored. The effect of the type and distribution of N atom species, i.e. pyridinic-N, pyrrolic-N or quaternary-N atoms on Pd NPs dispersion and also the stability of the Pd/N-CNTs was also investigated. The catalytic activity of the resulting Pd/N-CNTs catalysts was compared to that of Pd/CNTs in Suzuki coupling and solventfree benzyl alcohol oxidation reactions. Some comparisons were made with a few examples in the literature. Also, the recyclability of the synthesized heterogeneous catalysts was examined.

## Experimental

### Materials

Ferrocenecarboxaldehyde (98%) and benzophenone (99%) were supplied by Sigma-Aldrich. Palladium(II) acetyl acetate ( $\text{Pd}(\text{acac})_2$ ) (99%), acetonitrile (99%), benzyl alcohol (98%), sodium borohydride (95%) and benzaldehyde (99%) were obtained from Merck Chemicals. All organic substrates were purchased from Sigma-Aldrich with 98–99% purity and were used as received without further treatment. Double-deionized water was used throughout the experiments.

### Synthesis of 1-ferrocenylmethyl(2-methylimidazole) catalyst

The general procedure described by Pan et al. [46] was followed in the synthesis of 1-ferrocenylmethyl(2-methylimidazole). Briefly, ferrocenemethanol

(1 mM) and 2-methyl-1H-imidazole (1.1 mM) mixture was refluxed in acetic acid for 6 h at 60 °C. The reaction was monitored on preparative TLC, with hexane/diethyl ether (v/v 2:1, 10 mL) as the eluent. Upon completion, it was neutralized and washed with 50% KOH in distilled water to remove excess acetic acid. The residue was chromatographed on a silica-packed column with  $\text{CH}_2\text{Cl}_2/\text{MeOH}$  (4:1) as the eluent. Yield: 68%; IR ( $\text{cm}^{-1}$ ) 703.82, 730.95, 896.20, 1264.38, 1422.24, 3055;  $^1\text{H-NMR}$  spectra ( $\text{CDCl}_3$ ) 2.27 (3H, s,  $\text{CH}_3$ ), 4.12 (9H, m, Cp), 4.73 (2H, s,  $\text{CH}_2$ ), 6.73 (1H, s, imidazole), 6.81 (1H, s, imidazole);  $^{13}\text{C-NMR}$  spectra ( $\text{CDCl}_3$ ): d (ppm) = 13.13, 23.75, 29.69, 45.84, 68.79, 77.30, 82.78, 118.99, 126.43, 128.799, 130.87, 143.94. LC-MS ( $\text{C}_{10}\text{H}_{16}\text{FeN}_2$ ) EI:  $[\text{M} + \text{H}^+]$   $m/z$  calc. 280.10022, found 281.10015.

### Preparation of CNTs, N-CNTs and N-CNT-1%

CNTs were synthesized by dissolving ferrocene (0.25 g) in toluene (9.75 g) to make 10 g precursor solution, while N-CNTs were synthesized by pyrolyzing 1-ferrocenylmethyl(2-methylimidazole) (0.25 g) in acetonitrile (9.75 g) at 850 °C (CVD method). In the case of N-CNT-1% synthesis, this was done by a mixing 1-ferrocenylmethyl(2-methylimidazole) (0.25 g) and benzophenone (0.5 g) (oxygen source) in acetonitrile (9.25 g). The symbol 1% represents the weight percentage of oxygen from benzophenone in the reactant mixture. The CVD procedure and set-up were followed according to the procedure described in previous reports [47]. In a typical experiment, the reactant mixtures were injected by a syringe at a rate of  $0.8 \text{ mL min}^{-1}$  through the quartz tube placed in a muffle furnace. The mixture was swept through the tube by 10% hydrogen in argon carrier gas, at a rate of  $100 \text{ mL min}^{-1}$ . After 30 min of reaction, the furnace was cooled to room temperature, and the product was collected from the reactor. Before use, the samples were calcined at 300 °C for 3 h to remove amorphous carbon and chemically treated by refluxing in 6M  $\text{HNO}_3$  under vigorous stirring at 120 °C for 24 h. Afterwards, the samples were washed with double-distilled water followed by ethanol and then dried at 100 °C. The resulting fluffy and black carbon materials obtained without and with benzophenone were labelled N-CNTs and N-CNTs-1%, respectively, and were characterized by

TEM, SEM, SAED, XRD, Raman, ICP-OES, DSC/TGA and XPS.

### Preparation of Pd/CNT, Pd/N-CNTs and Pd/N-CNTs-1% catalysts

The MOCVD technique, as outlined by previous reports [48], was employed for 0.02 mol% Pd loading onto CNTs and N-CNTs support. Pd(acac)<sub>2</sub> (0.048 g) was mixed with 0.316 g of acid-treated CNTs, N-CNTs and N-CNTs-1%, followed by thorough grinding, using a pestle and mortar. The resulting mixture was transferred into a stainless steel MOCVD reactor. The sealed MOCVD reactor was evacuated with the aid of a vacuum pump maintained at a partial pressure of  $2.1 \times 10^{-2}$  mbar for 40 min. The MOCVD reactor was then inserted into a CVD muffle furnace and heated at 120 °C for 30 min. The temperature was then ramped up to 300 °C at a rate of 2 °C min<sup>-1</sup> and thereafter maintained at 300 °C for 45 min. The obtained samples were kept under ambient condition and stored under an inert atmosphere for further applications.

### Characterization

X-ray diffraction patterns were recorded on a Rigaku/D<sub>max</sub> RB using a graphite monochromatized high-density Cu K $\alpha$  radiation ( $\lambda = 0.15406$  Å). Fourier transform infrared (FTIR) was recorded by the use of KBr pellets with PerkinElmer spectrum RX1 FTIR spectrometer. Raman spectra were recorded on DeltaNu Advantage 532<sup>TM</sup> Raman spectrometer with a 1 mW laser power on the sample compartment. Spectra were obtained with five accumulations at 1 min each. Microstructure images were obtained by scanning electron microscopy (SEM) (JOEL JEM 1010) and transmission electron microscopy (TEM) (JOEL JSM 6100). Higher magnifications were obtained from high-resolution transmission electron microscope (HRTEM) operated at 200 kV. N<sub>2</sub> adsorption-desorption isotherms and surface area of CNTs and N-CNTs were determined on a Micromeritics Tristar II surface area analyser. The Pd content of the catalysts was determined by inductively coupled plasma-optical emission spectroscopy (ICP-OES) (PerkinElmer Optima 5300 DV). The thermal stabilities of CNTs and N-CNTs were measured using a Q Series<sup>TM</sup> thermal analyser DSC/TGA (Q600). The H<sub>2</sub>-TPR experiments were conducted in a gas mixture

containing 10% H<sub>2</sub> in Ar by Micromeritics Autochem II chemisorption analyser (2920) with the flow rate of 30 mL/min. X-ray photoelectron spectroscopy (XPS) analysis was carried out on a KRATOS AXIS Ultra DLD equipped with Al K $\alpha$  (1486 eV) X-rays, with X-ray power of 20 W and a beam diameter of 100  $\mu$ m. The CasaXPS programme was employed in the analysis of XPS data. Proton NMR spectra were recorded on a 400 MHz Bruker Ultrashield spectrometer at room temperature using deuterated CDCl<sub>3</sub> or DMSO as solvents. The Suzuki–Miyaura coupling reactions and solventfree oxidation of benzyl alcohol products were identified using GC-FID (Shimadzu 2010 gas chromatograph).

### General procedure for Suzuki reaction

In a typical Suzuki reaction, phenylboronic acid (2.5 mmol), aryl halide (2.5 mmol), Pd catalysts (20 mg), K<sub>2</sub>CO<sub>3</sub> (4 mmol) and EtOH–H<sub>2</sub>O (1:1, v/v, 10 mL) solvents were added into a round-bottom flask equipped with a stirrer. The reaction mixtures were stirred at 60 °C for 10–30 min under reflux. Upon reaction completion, the reaction product was cooled and filtered through a 0.22- $\mu$ m pore polycarbonate filter to separate the catalyst, and the filtrate was extracted with CH<sub>2</sub>Cl<sub>2</sub> (10 mL) three times. The organic layer fractions were combined into one conical flask and dried with anhydrous sodium sulphate. Thereafter, the mixture was filtered, and the residue was concentrated by flash chromatography on silica gel (0.0063–0.20 mm) with hexane/ethyl acetate (10:1) eluent, leading to isolation of pure biphenyl product.

### Solventfree oxidation of benzyl alcohol

The solventfree oxidation reactions of benzyl alcohol were carried out in a three-necked round-bottom flask (25 mL), pre-heated in an oil bath equipped with a condenser. Pd catalysts (20 mg) was added to benzyl alcohol (5.0 mL) and stirred at 500 rpm for each experiment. The mixture was heated under reflux at 110 °C for 3 h and flushed with pure oxygen at a flow rate of 20 mL/min. After the reaction, the products were cooled to room temperature and centrifuged to separate the catalysts. The products were analysed by a 30-m DB-1 capillary gas chromatography (GC) equipped with FID detector (Shimadzu 14B, FID detector) using n-dodecane as an internal

standard. The column temperature was kept at 100 °C for 10 min and then raised to 200 °C at a heating rate of 10 °C/min. The conversion of benzyl alcohol and selectivity towards benzaldehyde product was calculated after three consecutive runs. The turn over frequency (TOF) for each catalyst was calculated using Eq. (1).

$$\text{TOF} = \frac{\text{No. of moles of BZA}}{\text{No. of moles of active centres on catalyst} \times \text{time(h)}} \quad (1)$$

### Recycling and hot filtration leaching tests

After each catalytic cycle, the catalyst was firstly washed sufficiently with distilled water, sequentially with ethanol and acetone and then finally with dichloromethane before being dried at 110 °C for 24 h. Further catalytic reaction was carried out using the dried black residue. Hot filtration leaching test was carried out for the Suzuki reaction between iodobenzene (2.5 mmol) and phenylboronic acid (2.5 mmol) under optimized conditions. After 30 min, half of the reaction mixture was centrifuged and filtered while hot at 2000 rpm. The reaction was allowed to continue under stirring for another 6 h. Subsequently, the reaction yield of the unfiltered and the filtered solution was monitored by GC analysis after sampling at a predetermined time.

## Results and discussion

### Characterization of catalysts

The structural information and the crystalline phase of the catalysts were investigated using an X-ray diffractometer. Figure 1a shows the XRD pattern of Pd/CNTs, Pd/N-CNTs and Pd/N-CNTs-1%. All the catalyst showed the diffraction characteristic peaks of Pd NPs. The diffraction peak at 26.35° was indexed to the (002) crystal face reflection of the graphitic carbon in CNTs and N-CNTs, while the peaks at 40.00, 46.75 and 68.18° were attributed to the (111), (200) and (220), respectively, hexagonal close-packed crystalline phase of Pd face-centred cubic (fcc) structure in Pd/N-CNTs and Pd/CNTs [49].

The Pd NPs crystallite sizes were estimated from Pd (111) peaks using the Scherrer equation given in Eq. (2):

$$D = \frac{0.89\lambda}{\beta \cos \theta} \quad (2)$$

where  $D$  = average diameter of the Pd/NPs in nm,  $\lambda = 0.154$  nm (i.e. the wavelength of the X-rays),  $\theta$  = diffraction angle of the Pd (111) reflection and  $\beta$  = full width at half maximum (FWHM) of the Pd reflection plane. The lattice  $d$ -spacing calculated for the Pd (111) plane by Bragg's law for Pd/CNTs, Pd/N-CNTs and Pd/N-CNTs-1% was found to be 2.3152, 2.2530 and 2.3917 Å, respectively. According to the Scherrer's method, the full width at half maximum (FWHM) of the diffraction peak is inversely proportional to the particle size [50]. The calculated palladium nanoparticle sizes of Pd/CNTs, Pd/N-CNTs and Pd/N-CNTs-1% were 9.5, 3.1 and 7.5 nm, respectively. This trend is comparable with the nanoparticle size obtained from the TEM analysis (Table 1). The ICP-OES analysis of the catalysts gave approximately 0.02 mol% Pd loading for all catalysts (Table 1).

The carbon framework and structural defect instigated by N-doping was further evaluated quantitatively by the Raman spectroscopy (Fig. 1b). This was done to evaluate the degree of disordered carbon structure caused by a defect on the graphitic carbon sheets. An intense D-band peak at  $\sim 1348$   $\text{cm}^{-1}$  and G-band at  $\sim 1590$   $\text{cm}^{-1}$  are ascribed to the disordered carbon and the graphitic carbon, respectively [51]. The ratio of D- to G-band intensity ( $I_D/I_G$ ) was used to estimate the degree of distortions that exist in CNTs and N-CNTs. It was found that the ratio of  $I_D/I_G$  for Pd/CNTs (0.7583) was much less when compared to Pd/N-CNTs (0.9738) and Pd/N-CNTs-1% (0.8366). The lower  $I_D/I_G$  ratio demonstrates a more graphitic structure for Pd/CNTs, while on the other hand higher  $I_D/I_G$  ratio suggests a more successful N-doping in the increasing order of Pd/N-CNTs to Pd/N-CNTs-1%.

The SEM images of the Pd/N-CNTs showed a uniformly dispersed spherical Pd NPs indicative of a hierarchical porous network, often required in heterogeneous catalysis [52] (Fig. 2a). The morphology and the deposition of Pd NPs on CNTs and N-CNTs were clearly identified by the dark spots visible in Fig. 2b, c, respectively. Figure 2b, c shows a typical TEM and HRTEM images of Pd/N-CNTs-1%.

**Figure 1** **a** XRD diffraction pattern and **b** Raman spectra of Pd/CNTs, Pd/N-CNTs and Pd/N-CNTs-1% catalysts.

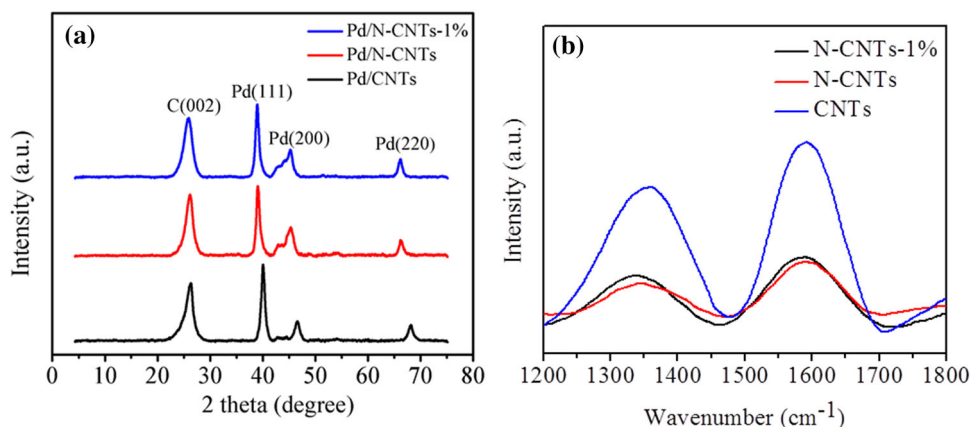
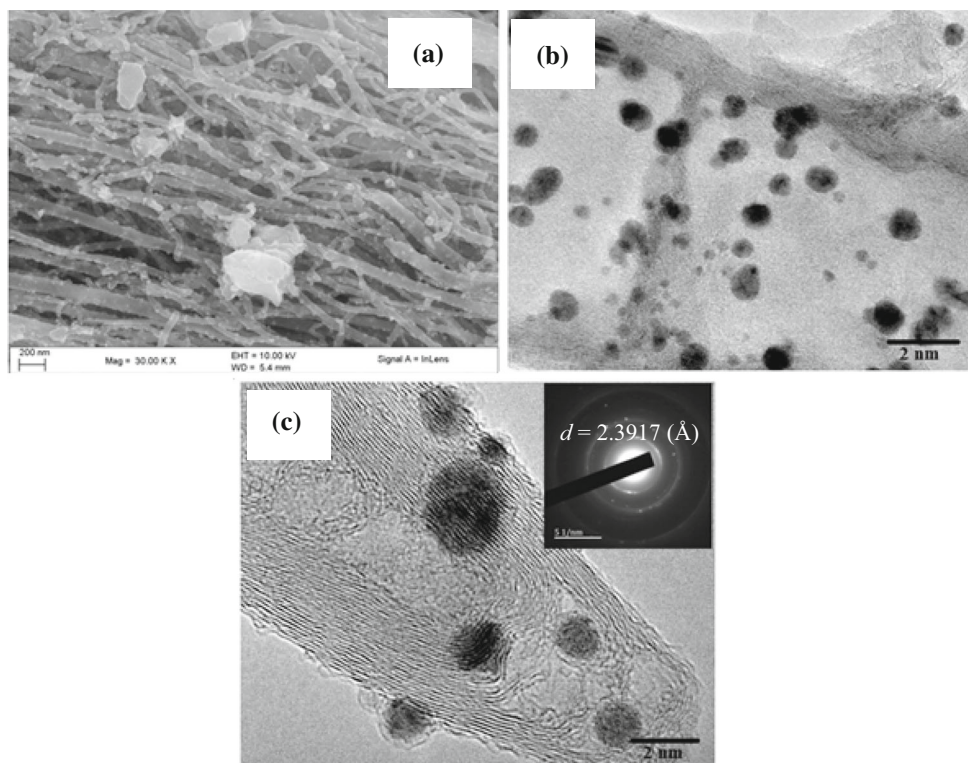


**Table 1** Properties of Pd/CNTs and Pd/N-CNTs catalysts based on ICP-OES, XRD and TEM

Entry	Catalyst	XRD			TEM $d_{\text{NP}}/\text{nm}^{\text{b}}$	(ICP-OES) Pd loading (mol%) <sup>c</sup>
		$d_{\text{NP}}/\text{nm}^{\text{a}}$	Interlayer spacing (Å)	FWHM of Pd (111) peak (°)		
1	Pd/N-CNTs	3.1	2.2530	0.2519	3.4	0.016
2	Pd/N-CNTs-1%	7.5	2.3917	0.2519	7.3	0.019
3	Pd/CNTs	9.10	2.3152	0.2340	8.7	0.017

<sup>a</sup> $d_{\text{NP}}$ —palladium nanoparticle diameter size determined by powdered XRD; <sup>b</sup> $d_{\text{NP}}$ —palladium nanoparticle diameter size determined by TEM; <sup>c</sup>mol% of Pd on N-CNTs determined by ICP-OES

**Figure 2** **a** SEM image of the Pd/N-CNTs-1%, **b** TEM image of Pd/N-CNTs-1% and **c** HRTEM image of Pd/N-CNTs-1%. Inset shows the matching SAED patterns.



TEM investigations revealed the average sizes to be 3.4, 7.3 and 8.7 nm, for CNTs, N-CNTs and N-CNTs-1%, respectively, and it also showed the distribution of the embedded Pd NPs. This result is consistent with particle sizes reported by Wang et al. [35]. Notably, the density of Pd NPs on N-CNTs-1% is profuse, and no nanoparticle aggregation is observed on the nanotube surface (Fig. 2b). The TEM result indicates that N-doping plays an essential role in Pd NPs dispersibility due to close interaction between Pd particles and defective N-CNTs than the graphitic CNTs [53]. The Pd atoms are deposited on the curvature of the wrinkled carbon sheets (Fig. 2c), suggestive of a functional interaction between Pd NP and N atom on N-CNT structure [53]. The crystallinity of Pd NPs anchored on the graphitic carbon was further determined by a selective area electron diffraction pattern (SAED, inset in Fig. 2c). The *d*-spacing (2.3917 Å) is consistent with the Pd (111) planes obtained from XRD analysis. Pd NPs consists of concentric rings, composed of bright discrete diffraction spots, which can be indexed to the (111), (200), (220) and (311) planes of fcc Pd. The SAED pattern of the as-prepared Pd nanoparticles shows their high crystallinity.

The chemical composition was investigated by FTIR (Fig. 3). The peaks at 2963 and 2843  $\text{cm}^{-1}$  characterize the stretching vibration of the  $\text{CH}_2$  and  $\text{CH}_3$  groups, respectively, present in all samples [54]. The bands at 1530 and 1307  $\text{cm}^{-1}$  are assigned to the  $\text{sp}^2$  C=C and aromatic C–N stretching bonds,

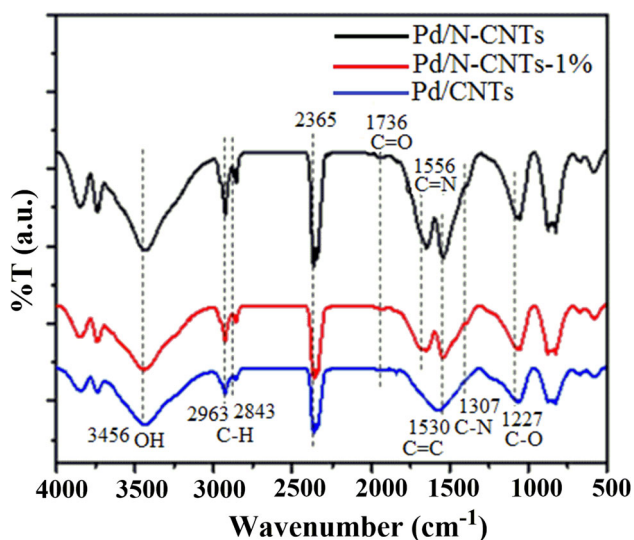


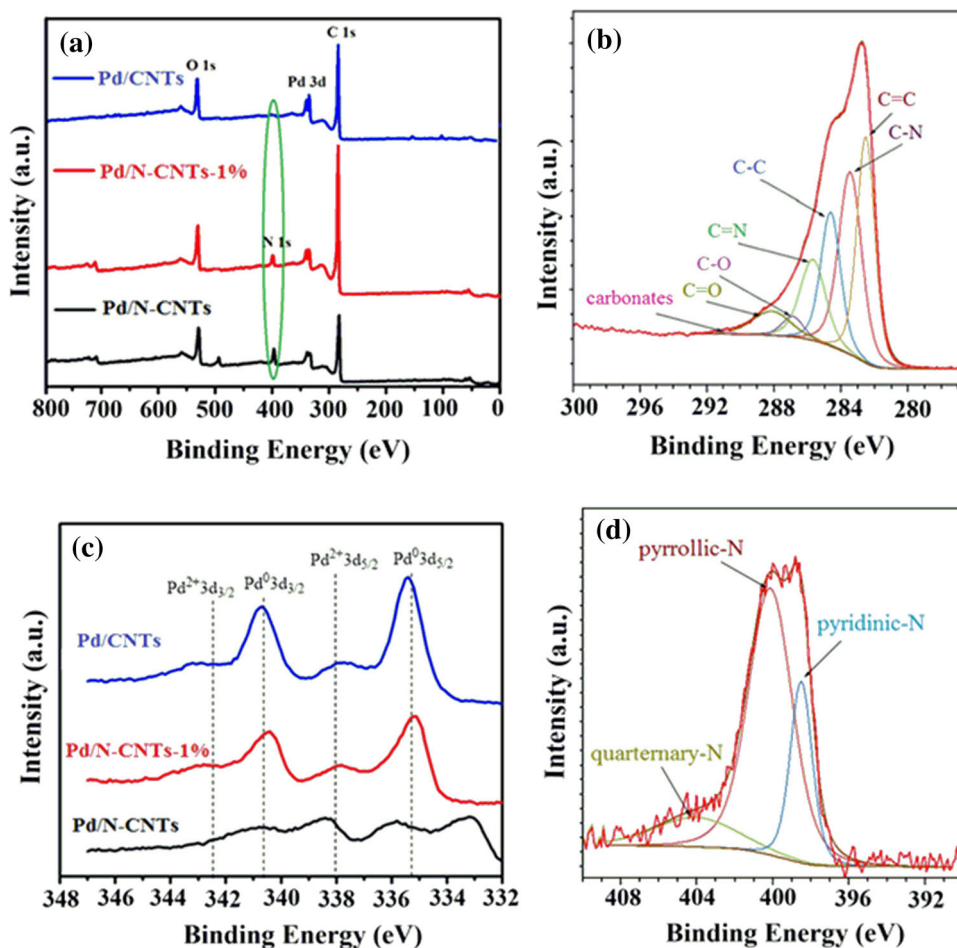
**Figure 3** FTIR spectra of Pd/CNTs, Pd/N-CNTs and Pd/N-CNTs-1%.

respectively [55]. The bands at 1736, 1556 and 1227  $\text{cm}^{-1}$  were assigned to C=O, C=N and C–O, respectively [56–58]. The peak observed at 2370  $\text{cm}^{-1}$  was assigned to trapped  $\text{CO}_2$  stretching and was observed in all samples [56, 59]. Compared with Pd/CNTs, the appearance of C=N and C–N functional groups in Pd/N-CNTs indicates the doping of N atom into the graphitic carbon.

The bulk composition of Pd/CNTs, Pd/N-CNTs and Pd/N-CNTs-1% catalysts was analysed with an X-ray photoelectron spectroscopy (XPS). The full spectra survey (Fig. 4a) revealed the presence of C, O and Pd in Pd/CNTs, while C, N, O and Pd were detected in Pd/N-CNTs. The percentage composition of all surface elements from XPS analysis is given in Supplementary Table S1. C 1s peaks were deconvoluted into five individual peaks as shown in Fig. 4. The robust signals C 1s confirmed the presence of oxygen functionalization on the CNTs and N-CNT surfaces. Figure 4b shows the peaks at 286.6 (C–O), 288.7 (O–C=O) and 290.2 eV (C–O–C), which are ascribed to the oxygen-containing moieties [45, 60, 61]. The peaks 284.3, 285.1, 287.1, 283.9 and 291.5 eV are assigned to  $\text{sp}^2$  C,  $\text{sp}^3$  C, C=N, C–N and carbonates, respectively.

The total nitrogen content on N-CNTs and N-CNT-1% was 10.56 and 6.92 at.%, respectively (Supplementary Table S1). A similar result was reported by Koos et al. [62], where nitrogen contents in N-CNTs decrease as N/C ratio decreases. The N 1s peaks of the high-resolution spectrum (Fig. 4d; Supplementary Figure S5) were deconvoluted to three symmetrical peaks assigned to pyridinic (398.4 eV), pyrrolic (400.1 eV) and oxidized nitrogen-like N-oxides of pyridinic-N (404.2 eV) which is typical of N-doped CNTs [63, 64]. The analysis of the N 1s spectra conformed with Kotakoski et al. [65] simulation, which suggested that at higher nitrogen atom concentration, N atom might be introduced as pentagon defect corresponding to pyrrolic-N type, while incorporation of a lower amount of nitrogen into the CNTs hexagonal structure was ascribed to pyridinic-N type [66]. Although most studies argue that the type of nitrogen functionalities and N-doping level can be controlled or rather depend on synthesis condition [67–70], the introduction of oxygen-containing benzophenone into the reaction mixture can lead to substantial increase in the pyrrolic-N. This can be attributed to the formation of  $\text{NO}_x$  resulting from the reaction of nitrogen with oxygen. On the other hand,

**Figure 4** **a** XPS survey scan spectra of the three Pd catalysts, **b** C 1s spectrum of Pd/N-CNT-0%, **c** Pd 3d spectrum of the three Pd catalysts and **d** N 1s spectrum of Pd/N-CNT-1%.



also the emergence of pyridinic oxides is a result of the conversion of quaternary-N. This occurs due to highly reactive oxidation reaction induced by the presence of benzophenone dissolved in the reaction mixture for N-CNTs-1% [71].

XPS analysis also showed the chemical state of Pd particles on CNTs and N-CNTs surface. The interaction of the pyrrolic nitrogen of N-CNTs and Pd NPs of different sizes showed pairs of doublet overlapping peaks in Pd 3d XPS spectra, corresponding to Pd 3d<sub>5/2</sub> and Pd 3d<sub>3/2</sub> (Fig. 4c). The Pd 3d peaks with binding energies at 335.6 eV (Pd<sub>5/2</sub>) and 340.6 eV (Pd<sub>3/2</sub>) [72, 73] were attributed to Pd<sup>0</sup>, while peaks at 337.7 eV (Pd<sub>5/2</sub>) and 342.7 eV (Pd<sub>3/2</sub>) [74] were related to Pd<sup>2+</sup> (Supplementary Table S2). The XPS data also revealed that Pd<sup>0</sup> was predominant on the surfaces of the three catalysts with no noticeable Pd<sup>2+</sup> ion, indicating that Pd<sup>2+</sup> ion was reduced to Pd NPs. The weak Pd<sup>2+</sup> peak observed at 336.3–336.9 eV was attributed to the formation of PdO due to sample exposure to air. The deposited Pd NPs were well

anchored on N-CNTs with an average size of 3.4 and 7.3 nm for N-CNTs and N-CNTs-1%, respectively. This could be attributed to the high nitrogen density on the N-CNTs surface and enhanced anchoring of the Pd NPs, making the catalysts less prone to agglomeration and sintering on cooling during catalyst synthesis. Following the peak area integration of Pd 3d peaks, the total molar fraction of Pd is ~ 76% for Pd/N-CNTs, while Pd/N-CNTs-1% had a lower value of 56%. Detailed XPS results are accessible in Supporting Information Table S1 and Table S2.

For N-CNTs, the decrease in the pyridinic-N concentration with increased pyrrolic-N was observed upon introduction of oxygen into the reaction mix (Fig. 5; Supplementary Table S1). It is noteworthy that pyrrolic-N species were 70% in Pd/N-CNTs-1%, with such N species acting as anchoring site, thereby enabling the nucleation and growth of metal nanoparticles [75]. From the results, the increased percentage of pyrrolic-N is due to the dilution of the nitrogen source which largely affects the N species



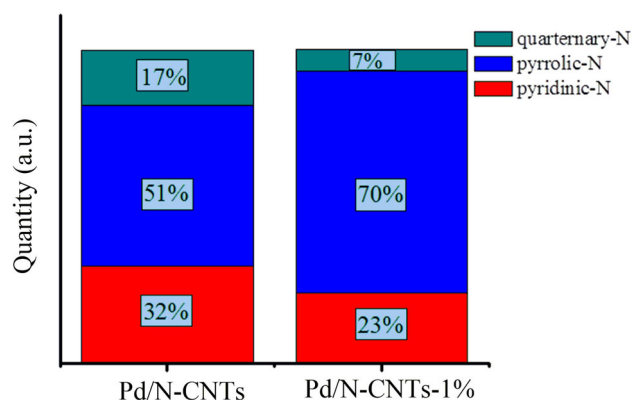


**Figure 5** Distribution of nitrogen species (%) present in Pd/N-CNTs and Pd/N-CNTs-1%.

formation [76, 77]. Also, the observed increase in pyrrolic-N concentration for N-CNTs-1% could be attributed to the decrease in  $N/C$  ratio in the reaction mixture as precursor decomposition is assumed to occur at the surface of Fe NPs (i.e. top-growth model) [78]. The formation of pyrrolic-N and pyridinic-N on the outer shell of N-CNTs is due to the interaction of NH and CN species on catalyst surface followed by their surface or subsurface diffusion [79].

The surface area properties of the synthesized Pd/CNTs, Pd/N-CNTs and Pd/N-CNTs-1% catalysts were obtained from  $N_2$  adsorption–desorption isotherms as given in Table 2 with the typical isotherm shown in Fig. 6a. All samples showed type IV isotherm curves [80] with an  $H_1$  hysteresis loop between 0.50 and 0.99 P/Po, typical of mesoporous and macroporous structured material with narrow pore size distribution associated with a cylindrical-like porous material such as CNTs [81]. The oxidation of the CNTs and N-CNTs via acid treatments led to the opening of tube ends, which upon deposition of Pd metal, these openings were blocked by nanoparticles, thereby inhibiting  $N_2$  adsorption. This results in a

**Table 2** Surface area of catalyst support used

Catalyst	$S_{BET}$ ( $m^2g^{-1}$ )	Pore volume distribution (nm)
CNT	135.42	0.434
N-CNTs	55.29	1.031
N-CNTs-1%	98.46	0.736
Pd/CNTs	133.87	0.402
Pd/N-CNTs	47.44	1.361
Pd/N-CNTs-1%	87.50	0.846

decrease in the surface area of Pd/CNTs ( $133.87 m^2g^{-1}$ ), Pd/N-CNTs ( $47.44 m^2g^{-1}$ ) and Pd/N-CNTs-1% ( $87.50 m^2g^{-1}$ ) catalysts [82, 83], relative to plain CNTs ( $135.42 m^2g^{-1}$ ), N-CNTs ( $55.29 m^2g^{-1}$ ) and N-CNTs-1% ( $98.46 m^2g^{-1}$ ), respectively. A significant increase in surface area was observed for N-CNTs-1% upon introduction of benzophenone in the reaction mixture, due to increase porosity caused by oxygen activation of the disordered N-CNTs.

Pd/N-CNTs showed the highest pore volume of 1.361 nm followed by Pd/N-CNTs-1% (0.846 nm) and Pd/CNTs (0.402 nm) (Fig. 6b), which could be associated with variation in reactant stoichiometry and post-synthesis functionalization [84, 85].

The strong interaction between CNTs (and N-CNTs) support and Pd NPs stabilization was investigated by  $H_2$ -TPR (Supplementary Figure S4). This interaction is evidenced by the reduction in temperature observed for the three catalysts in the  $H_2$ -TPR experiment. The position, width and intensity of the peaks depend significantly on the carbon material synthesis and pre-treatment of the supports. From the  $H_2$ -TPR profile, the hydrogen desorption peak at 50 °C could be attributed to interstitial Pd  $\beta$ -hydride. A sharp peak centred at 298 °C can be observed from Pd/CNTs and Pd/N-CNTs (Supplementary Fig. 4). The broad peak centred at 120 °C could be ascribed to the reduction of  $Pd^{2+}$  to  $Pd^0$  which is in support of observed results from the Pd 3d XPS spectra [86] (Fig. 5c).

## Catalytic performance

### Suzuki coupling reactions

A typical Suzuki coupling reaction was conducted using iodobenzene (2 mmol) and phenylboronic acid (2.5 mmol) as reactants, a base (4 mmol) and catalyst (20 mg). The solvent, base and temperature were varied to optimize the reaction conditions (Table 3). Table 3 summarizes the results obtained for quantitative yields of biphenyl compounds. High yields were obtained in protic solvents such as MeOH, EtOH and iPrOH (Table 3, entries 1, 2 and 12), while poor yields were obtained for aprotic solvents such as DMF, dioxane, acetonitrile and acetone (Table 3, entries 11 and 13–15). However, when  $H_2O$  was introduced as a solvent, a gradual increase in reactivity was observed relative to aprotic solvents

**Figure 6** **a** N<sub>2</sub> adsorption–desorption isotherms and **b** pore size distribution of Pd/CNTs, Pd/N-CNTs and Pd/N-CNT-1%.

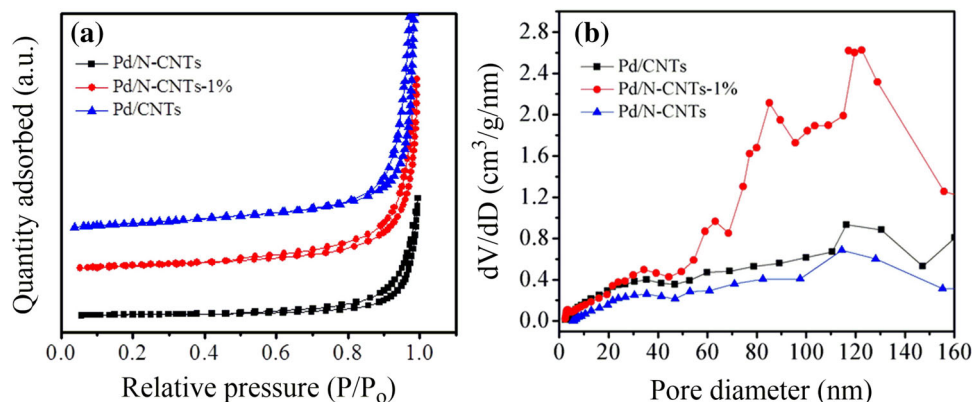


**Table 3** Screening of the reaction conditions for Suzuki cross-coupling reactions of phenylboronic acid with iodobenzene catalysed by Pd/N-CNTs

Entry	Solvents	Base	Temperature (°C)	Yield <sup>a</sup> (%)
1	MeOH	K <sub>2</sub> CO <sub>3</sub>	60	85
2	EtOH	K <sub>2</sub> CO <sub>3</sub>	60	86
3	H <sub>2</sub> O	K <sub>2</sub> CO <sub>3</sub>	60	59
4	H <sub>2</sub> O	K <sub>2</sub> CO <sub>3</sub>	100	65
5	THF–H <sub>2</sub> O (1:1, v/v)	K <sub>2</sub> CO <sub>3</sub>	80	46
6	EtOH–H <sub>2</sub> O (1:1, v/v)	K <sub>2</sub> CO <sub>3</sub>	60	98
7	EtOH–H <sub>2</sub> O (1:1, v/v)	NaOAc	60	80
8	EtOH–H <sub>2</sub> O (1:1, v/v)	Na <sub>2</sub> CO <sub>3</sub>	60	92
9	EtOH–H <sub>2</sub> O (1:1, v/v)	Et <sub>3</sub> N	60	82
10	EtOH–H <sub>2</sub> O (1:1, v/v)	K <sub>2</sub> PO <sub>4</sub>	70	67
11	DMF	K <sub>2</sub> CO <sub>3</sub>	80	27
12	iPrOH	K <sub>2</sub> CO <sub>3</sub>	80	82
13	Dioxane	K <sub>2</sub> CO <sub>3</sub>	80	26
14	CH <sub>3</sub> CN	NaOH	80	34
15	Acetone	K <sub>2</sub> CO <sub>3</sub>	80	46

Reaction conditions: iodobenzene (2 mmol) was reacted with phenylboronic acid (2.5 mmol) in the presence of a base (2 mmol) for 20 min, 20 mg of Pd/N-CNTs catalyst

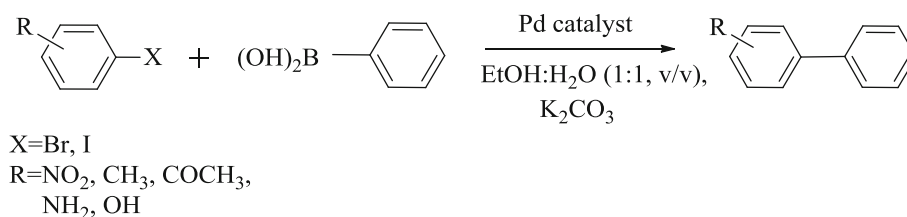
<sup>a</sup>Yields were calculated after isolation of the pure biphenyl compound through short-column chromatography using silica gel (100–200 mesh)

(Table 3, entry 3). An increase in the reactant solubility and reactivity was observed when solvent mixtures were employed (i.e. EtOH–H<sub>2</sub>O (1:1 v/v, 10 mL) and THF–H<sub>2</sub>O (1:1 v/v, 10 mL)) (Table 3, entries 5–10) similar to previous reports [87].

The advantage of the solvent mixture could be ascribed to the better solubility of the organic reactant in the organic base, which activates the phenylboronic acid and promotes reductive elimination reactions [88]. EtOH–H<sub>2</sub>O was found to be the solvent of choice than various bases such as K<sub>2</sub>CO<sub>3</sub>, NaOAc, KOH and Et<sub>3</sub>N. K<sub>2</sub>CO<sub>3</sub> produces better yields compared to Na<sub>2</sub>CO<sub>3</sub>, NaOAc and Et<sub>3</sub>N bases. This could be attributed to the partial homogeneity of K<sub>2</sub>CO<sub>3</sub> in the aqueous phase, leading to effective

activation of phenylboronic acid towards boronate complex formation [89]. The yield noticeably reduced from 92 to 82% for Na<sub>2</sub>CO<sub>3</sub> and Et<sub>3</sub>N, respectively (Table 3, entries 8 and 9).

Using the obtained optimum conditions, the catalytic efficiency of Pd catalysts in the coupling reaction between aryl halides (such as I and Br) and phenylboronic acid was investigated (Table 4). The reactions were rapid from 60 to 100 °C, beyond which an increase in the temperature did not increase the yield. Substituted aryl halide substrates with electron-withdrawing groups (–NO<sub>2</sub>, –COCH<sub>3</sub> and –CF<sub>3</sub>) and electron-donating groups (–CH<sub>3</sub>, –H and –NH<sub>2</sub>) produced good yields ranging from 73 to 98% of biphenyl compounds. The highest yield with

**Table 4** Catalytic performance of different supported Pd-based catalysts for Suzuki cross-coupling reaction under optimized conditions

Entry	Aryl halide	Time (min)	Yields <sup>a</sup> (%)		
			Pd/CNTs	Pd/N-CNTs	Pd/N-CNTs-1%
1	H-C <sub>6</sub> H <sub>4</sub> I	20	83	89	97
2	4-NO <sub>2</sub> -C <sub>6</sub> H <sub>4</sub> I	20	76	86	97
3	4-OH-C <sub>6</sub> H <sub>4</sub> I	15	65	82	94
4	4-CH <sub>3</sub> -C <sub>6</sub> H <sub>4</sub> I	20	58	65	92
5	4-COCH <sub>3</sub> -C <sub>6</sub> H <sub>4</sub> I	20	71	85	94
6	4-NH <sub>2</sub> -C <sub>6</sub> H <sub>4</sub> Br	20	83	86	98
7	H-C <sub>6</sub> H <sub>4</sub> Br	20	89	91	98
8	4-OH-C <sub>6</sub> H <sub>4</sub> Br	20	88	91	99
9	4-CH <sub>3</sub> -C <sub>6</sub> H <sub>4</sub> Br	20	86	92	93
10	4-NO <sub>2</sub> -C <sub>6</sub> H <sub>4</sub> Br	20	86	82	96
11	2-I-C <sub>6</sub> H <sub>4</sub> COOH	20	25	36	76
12	2-OH-C <sub>6</sub> H <sub>4</sub> Br	20	65	68	97
13	2-COCH <sub>3</sub> -C <sub>6</sub> H <sub>4</sub> Br	20	65	45	83
14	2-CF <sub>3</sub> -C <sub>6</sub> H <sub>4</sub> I	15	84	68	91

Reaction conditions: aryl halide (2 mmol), phenylboronic acid (2.5 mmol), K<sub>2</sub>CO<sub>3</sub> (4 mmol), catalyst (20 mg) and EtOH-H<sub>2</sub>O (1:1, v/v, 10 mL) at reflux 60 °C under air

<sup>a</sup>Isolated yields based on aryl halides. Under the equation, Pd catalyst refers to Pd/CNT, Pd/N-CNTs or Pd/N-CNTs-1% as catalyst used

substituted aryl bromide was obtained using Pd/N-CNTs-1% catalyst within 10–30 min (Table 4, entries 2–10). Effect of substituents on the aryl halide has been reported for Suzuki reactions [90]. The lower yield obtained for electron-withdrawing substituent (–COOH) which facilitates the rate-limiting oxidative reaction could be attributed to increased acidity in the reaction mixture [90] (Table 4, entry 11). The sterically hindered *ortho*-substituted 2-bromophenol and 2-iodobenzotrifluoride proceeded with good yields but not with excellent yields as obtained for *para*-substituted aryl halide (Table 4, entries 12 and 14). Among substituted aryl halides, substituted bromobenzene gave higher yields (Table 4, entry 10) than substituted iodobenzene (Table 4, entry 2), even though iodobenzene shows greater reactivity than bromobenzene due to iodine being a better leaving group. Nonetheless, there are known exceptions where reverse catalytic activity was observed for alkyl iodide as a substrate for Suzuki coupling

reactions. This could be attributed to the generation of iodide anion (I<sup>−</sup>) from alkyl iodide acting as a catalyst inhibitor during the catalytic reaction [91]. The excellent catalytic activity of Pd/N-CNTs-1% over Pd/N-CNTs and Pd/CNTs could be attributed to the smaller particles size of Pd NPs [92–94] and the strong interaction between Pd NPs and pyrrolic-N atom incorporated in the graphitic *sp*<sup>2</sup> carbon, thereby preventing Pd leaching and agglomeration. From the results of TEM sample measurements (from images obtained) and values calculated from Scherrer equation, XRD (Table 1), the order of Pd particle size on CNTs, N-CNTs and N-CNTs-1% supports follows the order Pd/CNTs < Pd/N-CNTs-1% < Pd/N-CNTs, respectively. The yield of biphenyls obtained follows the order Pd/CNTs < Pd/N-CNTs < Pd/N-CNTs-1%. The inconsistency in the particle size trend and the yield suggest that the Suzuki coupling reaction was influenced not only by the change in particle sizes but by other factors such as surface properties

and the nature of the support (amount of pyrrolic-N atom, XPS analysis) [33].

The efficiency of Pd/N-CNTs and Pd/N-CNTs-1% catalysts in this work is compared to those reported elsewhere for Suzuki coupling reactions of bromobenzene and phenylboronic acid [37, 38]. Table 5 shows that all reactions proceeded with better yields (> 90%) except a few with harsh reaction conditions and longer reaction times. From BET analysis, the surface area of Pd/CNTs, Pd/N-CNTs and Pd/N-CNTs-1% catalysts follows the order Pd/CNTs > Pd/N-CNTs-1% > Pd/N-CNTs. However, it was found that the yield of biphenyl follows the order Pd/CNTs < Pd/N-CNTs < Pd/N-CNTs-1%. This suggests that the coupling reaction is dependent not only of the surface area but also other factors such as surface properties including the pore volume [95, 96] and the nature of the support (amount of pyrrolic-N atom) [33].

### Solventfree benzyl alcohol oxidation reactions

In our study, we extend the application of Pd/CNTs, Pd/N-CNTs and Pd/N-CNTs-1% catalysts in the solventfree oxidation reaction of benzyl alcohol. The catalytic activities of the Pd catalysts in the oxidation of benzyl alcohol in pure oxygen with a flow rate of 20 mL/min at a temperature of 110 °C were investigated. A blank reaction without any catalyst was conducted. A lower conversion of 3% (Table 6) was obtained, confirming that the reaction could not proceed in the absence of a catalyst. Also, the use of CNTs and N-CNTs as catalysts produced noticeable

conversions of 15 and 35%, respectively (Fig. 7a). The oxidation reaction continued progressively as the catalytic activities increased in the order Pd/N-CNTs-1% > Pd/N-CNTs > Pd/CNTs, which correlates with an increase in the pyrrolic-N atom as observed in the XPS results. This increased catalytic activity is attributable to the effective enhancement of active surface oxygen by Pd NPs. For Pd/N-CNTs-1% and Pd/N-CNTs, about 98 and 96% conversion was achieved after 2 h of reaction, respectively, with a high TOF (Table 6). Nonetheless, a lower conversion was obtained for Pd/CNTs which could be due to the resulting agglomeration of Pd NPs which led to unfavourable larger Pd NPs size. The selectivity of Pd/N-CNTs-OT catalyst (96%) was found to be superior to Pd/N-CNTs which is reported in the literature [35] with larger particle size (Table 7, entries 5 and 7).

The catalytic strength of our catalyst for benzyl alcohol oxidation is comparable to other reported Pd-catalysed reactions (Table 7). The low selectivity observed for Pd/CNTs, Pd/N-CNTs and Pd/N-CNTs-1% catalysts after 30 min of reaction (Fig. 7b) is a result of (1) initial hydrogenolysis of benzyl alcohol towards the formation of toluene and (2) parallel oxidation reaction between benzyl alcohol and hydrogen [30]. However, further reaction of oxygen with hydrogen suppresses the hydrogenolysis reaction, thereby enhancing selectivity towards benzaldehyde formation after 120 min.

**Table 5** Catalytic performances of some Pd-based catalysts for Suzuki coupling of bromobenzene and phenylboronic acid

Entry	Catalyst	Reaction conditions (solvent, base, temp, time, Pd loading)	Yield (%)	TOF (h <sup>-1</sup> )	Refs.
1	CMC-NHC-Pd	EtOH-H <sub>2</sub> O, K <sub>2</sub> CO <sub>3</sub> , 60 °C, 3 h, 0.8 mol%	96	120	[97]
2	MOF-NPC-Pd	EtOH-H <sub>2</sub> O, K <sub>2</sub> CO <sub>3</sub> , 78 °C, 1 h, 0.1 mol%	98.6	–	[98]
3	Pd-rGO	EtOH-H <sub>2</sub> O, NaOH, 60 °C, 24 h, 0.5 mol%	5	0.4	[99]
4	Schiff base-MCNT-Pd	EtOH-H <sub>2</sub> O, K <sub>2</sub> CO <sub>3</sub> , r.t, 1 h, 0.2 mol%	98	–	[100]
5	G-MWCNTs-Pd	EtOH-H <sub>2</sub> O, K <sub>2</sub> CO <sub>3</sub> , 60 °C, 1 h, 0.5 mol%	95	799	[87]
6	Isoniazole-MWCNT-Pd	EtOH-H <sub>2</sub> O, K <sub>2</sub> CO <sub>3</sub> , 60 °C, 2 h, 0.2 mol%	98	–	[101]
7	Pd/CNT	H <sub>2</sub> O, Na <sub>2</sub> CO <sub>3</sub> , 80 °C, 24 h, 0.01 mol%	97	40	[102]
8	Pd@PANI	EtOH, K <sub>2</sub> CO <sub>3</sub> , 78 °C, 24 h, 0.12 mol%	76	–	[103]
9	Pd/N-CNTs	EtOH-H <sub>2</sub> O, K <sub>2</sub> CO <sub>3</sub> , 60 °C, 0.25 h, 0.02 mol%	91	2050	This work
10	Pd/N-CNTs-1%	EtOH-H <sub>2</sub> O, K <sub>2</sub> CO <sub>3</sub> , 60 °C, 0.25 h, 0.02 mol%	98	1068	This work

**Table 6** Catalytic performance of Pd/CNTs and Pd/N-CNTs catalyst in solventfree selective oxidation of benzyl alcohol

Samples	Conversion (%)	Selectivity (%)	TOF(h <sup>-1</sup> )
No catalyst	< 3	< 4	–
CNTs	15 ± 0.8	85 ± 2.7	247
N-CNTs	38 ± 2.6	94 ± 1.9	614
Pd/CNTs	85 ± 1.8	65 ± 0.2	9349.5
Pd/N-CNTs	96 ± 0.2	80 ± 0.1	10560
Pd/N-CNTs-1%	98 ± 0.1	96 ± 0.5	10780

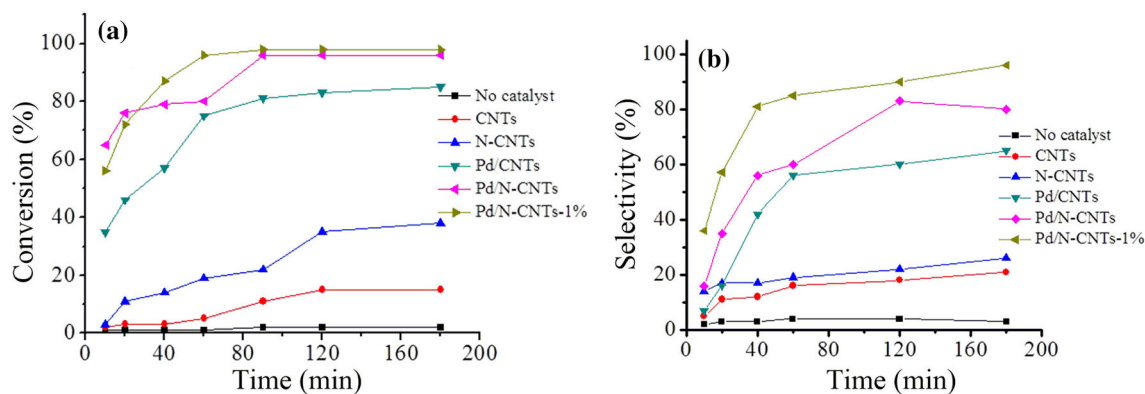
Reactions condition: 5 mL benzyl alcohol, 110 °C, 3 h, 50 mg catalyst, molecular O<sub>2</sub>. Conversion = mmol (benzyl alcohol) converted/mmol (initial benzyl alcohol) × 100%. Selectivity of benzaldehyde (%) = measured [benzaldehyde]/measured [benzyl alcohol converted] + measured [other products] × 100%

### Influence of the catalyst preparation conditions on catalytic performance

From our experiments, it has been shown that N-CNTs and N-CNTs-1% are more efficient support than CNTs for Pd-catalysed reactions. For N-CNT, nitrogen atom usually increases the electron density on metal catalysts, thereby providing a suitable site for anchoring [71], leading to better dispersion and ultimately facilitating the adsorption of reactant and desorption of products [108–110]. The lone pair bonding electron and higher electronegativity of the substituted N atoms within the carbon support enhance the support basicity, hence promoting the desorption of nitrogen at low temperature [111]. Also, nitrogen doping modifies the Pd NPs active sites. During catalyst preparation, active Pd NPs crystallites react with both the pyrrolic- and the pyridinic-N atoms on nanotubes surfaces. We also presume that nitrogen atoms are uniformly spread inside the nanotubes.

The introduction of oxygen during the carbon support synthesis and chemical functionalization offers great opportunities in tailoring the surface properties of these materials with better porosity, thereby enhancing diffusion and mass transfer of substrates during catalytic reactions [112]. The presence of hydrogen decreases the amount of N atoms doped on CNTs due to the reaction of N and H radicals to form NH<sub>3</sub> and HCN gases [113]. We, therefore, concluded that oxygen played a vital role by improving the nanotubes' quality by scavenging the H radicals via the reaction (i.e. H + O<sub>2</sub> → OH + O), as evidenced by the presence of a strong OH band obtained for N-CNTs-1% from the FTIR analysis (Fig. 4). The formation of OH radicals subsequently helps to suppress carbon etching at the growing edges, remove amorphous carbon (i.e. C + O → CO + O → CO<sub>2</sub>) and limit the supersaturation of carbon molecule during N-CNTs growth.

Surface properties of the CNTs and N-CNTs can be influenced by the amount of C–O functional group and the metal particle size. The Pd NPs size distribution on CNTs, N-CNTs and N-CNTs-1% is shown in Supplementary Figure S1. The Pd NPs size on the carbon materials follows the order: Pd/CNTs > Pd/N-CNTs > Pd/N-CNTs-1%. N-CNTs-1% produce good Pd particle dispersion due to the presence of a carbonyl functional group on the carbon surface. This was confirmed by O 1s peak of the three fitted components in the samples, namely: quinone and carbonyl group (C=O, 531.15 eV) [114]; ether and hydroxyl oxygen (C–O, 533.4 eV) [115, 116]; and carboxylic group oxygen (COOH, 534.4 eV) [117] from the XPS analysis. The increase in oxygen-containing fractions follows the trend: Pd/CNTs (11.37 at.%) < Pd/N-CNTs (12.72 at.%) < Pd/N-CNTs-1%

**Figure 7** Conversion (a) and selectivity (b) of benzyl alcohol over CNTs, N-CNTs, Pd/CNTs, Pd/N-CNTs and Pd/N-CNTs-1% catalysts.

**Table 7** Catalytic performances of benzyl alcohol oxidation over Pd catalysts

Entry	Catalyst	Pd loaded (wt%)	Time (h)	Conv. (%)	Sel. (%)	TOF (h <sup>-1</sup> )	Refs.
1	Pd-NC-ZS/10t	3	4	64	> 99	–	[104]
2	Pd/MagSBA	3	9	71	83.2	633	[105]
3	Pd/CNTs	1	1	17	91.3	1691	[30]
4	Pd@PBFS-500	1	0.5	87	> 99	690	[106]
5	Pd/N-CNTs	9	3	57	85	–	[35]
6	Pd/AC	1	3	18	91	30	[107]
7	Pd/N-CNTs	5	3	98	38	–	[35]
8	Pd/N-CNTs	5	3	96	96	10560	This work
9	Pd/N-CNTs-1%	5	3	98	> 99	10780	This work

(18.22 at.%). According to the FTIR and XPS results, carboxyl groups on the surface of N-CNTs-OT were capable of interacting with Pd NPs via covalent bonding [95]. Hence, the Pd/N-CNTs-OT catalyst played a critical role in preventing Pd NPs from leaching during the Suzuki coupling reaction and also in the solventfree benzyl alcohol oxidation, and this is due to the available binding sites (i.e. O–C=O, C–N, and C–O–C groups) available in N-CNTs-OT carbon support.

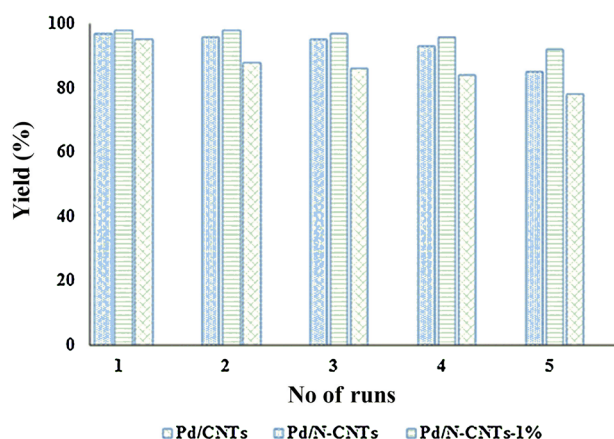
### Catalyst recyclability

The catalytic activities of the three catalysts were studied under the optimized conditions. The recyclability of the catalysts was investigated for iodobenzene and phenylboronic acid as a test substrate by filtration, and the results are illustrated in Fig. 8. The catalysts were washed with ethanol and subsequently with acetone and dichloromethane and dried overnight in an oven at 373 K after each run. The catalytic properties of the three catalysts remained unchanged until after the fifth runs, with no loss in their selectivity and activity. The Pd/CNTs become less active with a drop in yield to 84% after the fourth run, while Pd/N-CNTs and Pd/N-CNTs-1% showed the highest stability with a 93% yield after the fifth run. Further TEM analysis of the catalysts after five runs showed well-dispersed Pd NPs (Supplementary Figure S5) with minimal agglomeration. Table 8 shows the recyclability of the catalyst after seven runs for benzyl alcohol oxidation. The Pd/N-CNTs-1% catalyst produced an outstanding conversion of 96% after seven recycles of reaction regeneration, signifying even Pd NPs dispersion, high stability and robust interaction between carbon

support and Pd NPs, thus preventing not only agglomeration but also leaching.

### Pd leaching test

Leaching of metal NPs is of great concern in heterogeneous catalysis, and to confirm the amount of metal leached, the hot filtration test method was employed to investigate whether the Pd/CNTs and Pd/N-CNTs acted as heterogeneous catalysts. Similar catalyst amounts and reaction conditions for Suzuki reaction were employed for the hot filtration experiment. After 20 min of reaction, the catalyst was filtered, and the filtrate was analysed through ICP-OES. For the reaction, 36% conversion was recorded, and no trace of Pd species was detected. The reaction was allowed to proceed until after 120 min. It was observed that the reaction was halted after catalyst removal, indicating no further conversion (Supplementary Figure S6). We suggested that Pd species from Pd/N-CNTs-1% catalyst remain active in the

**Figure 8** Recyclability of Pd catalysts for Suzuki coupling reactions.

**Table 8** Reusability of the Pd/N-CNTs-1% catalyst for the oxidation of benzyl alcohol

Runs	1	2	3	4	5	6	7
Yields	96	96	96	96	95	95	92

catalytic cycle (i.e. oxidative addition, transmetalation and reductive elimination) of Suzuki reaction (Supplementary Figure S7), thus preventing catalyst loss and permitting easy recovery. The observed stability, catalytic efficiency and reusability of Pd/N-CNTs and Pd/N-CNTs-1% catalyst make them a suitable candidate for C–C coupling reactions and oxidation reactions.

Further ICP-OES analysis was carried out after the fifth run with 4.56 wt% Pd content recorded for Pd/N-CNTs and Pd/N-CNTs-1%, indicating a strong interaction of Pd NPs with the active sites of the carbon support thereby thwarting leaching. A combination of the results of recyclability and the hot filtration test showed that the catalyst is genuinely heterogeneous and selective towards Suzuki coupling and oxidation of benzyl alcohol reactions without significant Pd leaching.

## Conclusion

Pd/CNTs, Pd/N-CNTs and Pd/N-CNTs-1% catalysts were successfully synthesized by MOCVD techniques. Pd NPs sizes of 3.4, 7.3 and 8.7 nm were well dispersed on N-CNTs, N-CNTs-1% and CNTs, respectively. The catalysts possessed mesoporous surfaces with reasonable stability and excellent durability. The correlation of metal–carbon interaction, particle size distribution and the effect of pyrrolic-N atoms towards excellent catalytic activity and selectivity of Pd/N-CNTs-1% was successfully archived for Suzuki coupling and benzyl alcohol oxidation reactions. It must be stressed that 1% weight of oxygen atom, introduced by benzophenone, and seen from XPS result of Pd/N-CNTs-1%, is useful for applications where strong interfacial bonding of Pd NPs with carbon support is required.

## Acknowledgements

This research was financially supported by the National Research Foundation (NRF) South Africa,

Grant Number 103979. We are grateful to the School of Chemistry and Physics, University of KwaZulu-Natal (UKZN), for creating a conducive research laboratory for this work. Ayomide is grateful to Mrs Rashidat Labulo and Dr Moses Ollengo for proof-reading this manuscript.

## Compliance with ethical standards

**Conflict of interest** The authors declared that they have no conflict of interest.

**Electronic supplementary material:** The online version of this article (<https://doi.org/10.1007/s10853-018-2748-8>) contains supplementary material, which is available to authorized users.

## References

- [1] Harada T, Ikeda S, Hashimoto F, Sakata T, Ikeue K, Torimoto T et al (2010) Catalytic activity and regeneration property of a Pd nanoparticle encapsulated in a hollow porous carbon sphere for aerobic alcohol oxidation. *Langmuir* 26:17720–17725
- [2] Koltunov KY, Walspurger S, Sommer J (2004) Superacid and H-zeolite mediated reactions of benzaldehyde with aromatic compounds and cyclohexane. The role of mono- and dicationic intermediates. *Catal Lett* 98:89–94
- [3] Della Pina C, Falletta E, Rossi M (2008) Highly selective oxidation of benzyl alcohol to benzaldehyde catalyzed by bimetallic gold–copper catalyst. *J Catal* 260:384–386
- [4] Canellas E, Aznar M, Nerin C, Mercea P (2010) Partition and diffusion of volatile compounds from acrylic adhesives used for food packaging multilayers manufacturing. *J Mater Chem* 20:5100–5109
- [5] Siebel A, Gorlin Y, Durst J, Proux O, Fdr Hasché, Tromp M et al (2016) Identification of catalyst structure during the hydrogen oxidation reaction in an operating PEM fuel cell. *ACS Catal* 6:7326–7334
- [6] Goszewska I, Giziński D, Zienkiewicz-Machnik M, Lisovytiskiy D, Nikiforov K, Masternak J et al (2017) A novel nano-palladium catalyst for continuous-flow chemoselective hydrogenation reactions. *Catal Commun* 94:65–68
- [7] Saito Y, Ishitani H, Ueno M, Kobayashi S (2017) Selective hydrogenation of nitriles to primary amines catalyzed by a polysilane/SiO<sub>2</sub>-supported palladium catalyst under continuous-flow conditions. *ChemistryOpen* 6:211–215

- [8] Choudhary H, Jia J, Nishimura S, Ebitani K (2017) Surfactant-assisted Suzuki–Miyaura coupling reaction of unreactive chlorobenzene over hydrotalcite-supported palladium catalyst. *Asian J Org Chem* 6:274–277
- [9] Kim Y-O, You JM, Jang H-S, Choi SK, Jung BY, Kang O et al (2017) Eumelanin as a support for efficient palladium nanoparticle catalyst for Suzuki coupling reaction of aryl chlorides in water. *Tetrahedron Lett* 22:2149–2152
- [10] Choi J, Chan S, Yip G, Joo H, Yang H, Ko FK (2016) Palladium-zeolite nanofiber as an effective recyclable catalyst membrane for water treatment. *Water Res* 101:46–54
- [11] Choudhary M, Siwal S, Nandi D, Mallick K (2016) Catalytic performance of the in situ synthesized palladium–polymer nanocomposite. *New J Chem* 40:2296–2303
- [12] Gholinejad M, Bahrami M, Nájera C (2017) A fluorescence active catalyst support comprising carbon quantum dots and magnesium oxide doping for stabilization of palladium nanoparticles: Application as a recoverable catalyst for Suzuki reaction in water. *Mol Catal* 433:12–19
- [13] Freakley SJ, He Q, Harray JH, Lu L, Crole DA, Morgan DJ et al (2016) Palladium-tin catalysts for the direct synthesis of H<sub>2</sub>O<sub>2</sub> with high selectivity. *Science* 351:965–968
- [14] Labulo AH, Martincigh BS, Omondi B, Nyamori VO (2017) Advances in carbon nanotubes as efficacious supports for palladium-catalysed carbon–carbon cross-coupling reactions. *J Mater Sci* 52:9225–9248. <https://doi.org/10.1007/s10853-017-1128-0>
- [15] Yue D, Liu Y, Shen Z, Zhang L (2006) Study on preparation and properties of carbon nanotubes/rubber composites. *J Mater Sci* 41:2541–2544. <https://doi.org/10.1007/s10853-006-5331-7>
- [16] Salvétat J-P, Bonard J-M, Thomson N, Kulik A, Forro L, Benoit W et al (1999) Mechanical properties of carbon nanotubes. *Appl Phys A* 69:255–260
- [17] Nam DH, Cha SI, Lee KM, Jang JH, Park HM, Lee JK et al (2016) Thermal properties of carbon nanotubes reinforced aluminum-copper matrix nanocomposites. *J Nanosci Nanotechnol* 16:12013–12016
- [18] Qiu H, Shi Z, Guan L, You L, Gao M, Zhang S et al (2006) High-efficient synthesis of double-walled carbon nanotubes by arc discharge method using chloride as a promoter. *Carbon* 44:516–521
- [19] Prasek J, Drbohlavova J, Chomoucka J, Hubalek J, Jasek O, Adam V et al (2011) Methods for carbon nanotubes synthesis. *J Mater Chem* 21:15872–15884
- [20] Maruyama T, Kondo H, Ghosh R, Kozawa A, Naritsuka S, Iizumi Y et al (2016) Single-walled carbon nanotube synthesis using Pt catalysts under low ethanol pressure via cold-wall chemical vapor deposition in high vacuum. *Carbon* 96:6–13
- [21] Zheng C, Huang L, Zhang H, Sun Z, Zhang Z, Zhang G-J (2015) Fabrication of ultrasensitive field-effect transistor DNA biosensors by a directional transfer technique based on CVD-grown graphene. *ACS Appl Mater Interfaces* 7:16953–16959
- [22] Chen D, Holmen A, Sui Z, Zhou X (2014) Carbon mediated catalysis: a review on oxidative dehydrogenation. *Chin J Catal* 35:824–841
- [23] Meemken F, Baiker A (2017) Recent progress in heterogeneous asymmetric hydrogenation of C=O and C=C bonds on supported noble metal catalysts. *Chem Rev* 117:11522–11569
- [24] Martin-Martinez M, Ribeiro RS, Machado BF, Serp P, Morales-Torres S, Silva AM et al (2016) Role of nitrogen doping on the performance of carbon nanotube catalysts: a catalytic wet peroxide oxidation application. *Chem-CatChem* 8:2068–2078
- [25] Florea I, Ersen O, Arenal R, Ihiwakrim D, Messaoudi Cd, Chizari K et al (2012) 3D analysis of the morphology and spatial distribution of nitrogen in nitrogen-doped carbon nanotubes by energy-filtered transmission electron microscopy tomography. *J Am Chem Soc* 134:9672–9680
- [26] Xia W (2016) Interactions between metal species and nitrogen-functionalized carbon nanotubes. *Catal Sci Technol* 6:630–644
- [27] Old DW, Wolfe JP, Buchwald SL (1998) A highly active catalyst for palladium-catalyzed cross-coupling reactions: room-temperature Suzuki couplings and amination of unactivated aryl chlorides. *J Am Chem Soc* 120:9722–9723
- [28] Heidenreich RG, Krauter JG, Pietsch J, Köhler K (2002) Control of Pd leaching in Heck reactions of bromoarenes catalyzed by Pd supported on activated carbon. *J Mol Catal A: Chem* 182:499–509
- [29] Kim E, Jeong HS, Kim BM (2014) Studies on the functionalization of MWNTs and their application as a recyclable catalyst for C–C bond coupling reactions. *Catal Commun* 46:71–74
- [30] Yan Y, Jia X, Yang Y (2016) Palladium nanoparticles supported on CNT functionalized by rare-earth oxides for solventfree aerobic oxidation of benzyl alcohol. *Catal Today* 259:292–302
- [31] Maniam KK, Chetty R (2015) Electrochemical synthesis of palladium dendrites on carbon support and their enhanced electrocatalytic activity towards formic acid oxidation. *J Appl Electrochem* 45:953–962
- [32] He L, Weniger F, Neumann H, Beller M (2016) Synthesis, characterization, and application of metal nanoparticles supported on nitrogen-doped carbon: catalysis beyond electrochemistry. *Angew Chem Int Ed* 55:12582–12594



- [33] Ombaka LM, Ndungu PG, Kibet J, Nyamori VO (2017) The effect of pyridinic-and pyrrolic-nitrogen in nitrogen-doped carbon nanotubes used as support for Pd-catalyzed nitroarene reduction: an experimental and theoretical study. *J Mater Sci* 52:10751–10765. <https://doi.org/10.1007/s10853-017-1241-0>
- [34] Ding Y, Zhang L, Wu K-H, Feng Z, Shi W, Gao Q et al (2016) The influence of carbon surface chemistry on supported palladium nanoparticles in heterogeneous reactions. *J Colloid Interface Sci* 480:175–183
- [35] L-l Wang, L-p Zhu, N-c Bing, L-j Wang (2017) Facile green synthesis of Pd/N-doped carbon nanotubes catalysts and their application in Heck reaction and oxidation of benzyl alcohol. *J Phys Chem Solids* 107:125–130
- [36] Li M, Xu F, Li H, Wang Y (2016) Nitrogen-doped porous carbon materials: promising catalysts or catalyst supports for heterogeneous hydrogenation and oxidation. *Catal Sci Technol* 6:3670–3693
- [37] Zhang L, Dong W-H, Shang N-Z, Feng C, Gao S-T, Wang C (2016) N-Doped porous carbon supported palladium nanoparticles as a highly efficient and recyclable catalyst for the Suzuki coupling reaction. *Chin Chem Lett* 27:149–154
- [38] Zuo P, Duan J, Fan H, Qu S, Shen W (2018) Facile synthesis high nitrogen-doped porous carbon nanosheet from pomelo peel and as catalyst support for nitrobenzene hydrogenation. *Appl Surf Sci* 435:1020–1028
- [39] Ding S, Zhang C, Liu Y, Jiang H, Chen R (2017) Selective hydrogenation of phenol to cyclohexanone in water over Pd@ N-doped carbons derived from ZIF-67: role of dicyandiamide. *Appl Surf Sci* 425:484–491
- [40] Deng D-S, Han G-Q, Zhu X, Xu X, Gong Y-T, Wang Y (2015) Selective hydrogenation of unprotected indole to indoline over N-doped carbon supported palladium catalyst. *Chin Chem Lett* 26:277–281
- [41] Ombaka LM, Ndungu PG, Nyamori VO (2015) Pyrrolic nitrogen-doped carbon nanotubes: physicochemical properties, interactions with Pd and their role in the selective hydrogenation of nitrobenzophenone. *RSC Adv* 5:109–122
- [42] Chizari K, Janowska I, Houllé M, Florea I, Ersen O, Romero T et al (2010) Tuning of nitrogen-doped carbon nanotubes as catalyst support for liquid-phase reaction. *Appl Catal A Gen* 380:72–80
- [43] Amama PB, Pint CL, McJilton L, Kim SM, Stach EA, Murray PT et al (2008) Role of water in super growth of single-walled carbon nanotube carpets. *Nano Lett* 9:44–49
- [44] Futaba DN, Hata K, Namai T, Yamada T, Mizuno K, Hayamizu Y et al (2006) 84% catalyst activity of water-assisted growth of single walled carbon nanotube forest characterization by a statistical and macroscopic approach. *J Phys Chem B* 110:8035–8038
- [45] Duan X, Xiao M, Liang S, Zhang Z, Zeng Y, Xi J et al (2017) Ultrafine palladium nanoparticles supported on nitrogen-doped carbon microtubes as a high-performance organocatalyst. *Carbon* 119:326–331
- [46] He P, Du Y, Wang S, Cao C, Wang X, Pang G et al (2013) Synthesis, structure, and reactivity of ferrocenyl-NHC palladium complexes. *Z Anorg Allg Chem* 639:1004–1010
- [47] Oosthuizen RS, Nyamori VO (2012) Heteroatom-containing ferrocene derivatives as catalysts for MWCNTs and other shaped carbon nanomaterials. *Appl Organomet Chem* 26:536–545
- [48] Naidoo Q-L, Naidoo S, Petrik L, Nechaev A, Ndungu P (2012) The influence of carbon based supports and the role of synthesis procedures on the formation of platinum and platinum-ruthenium clusters and nanoparticles for the development of highly active fuel cell catalysts. *Int J Hydrogen Energy* 37:9459–9469
- [49] Saleh TA (2011) The influence of treatment temperature on the acidity of MWCNT oxidized by HNO<sub>3</sub> or a mixture of HNO<sub>3</sub>/H<sub>2</sub>SO<sub>4</sub>. *Appl Surf Sci* 257:7746–7751
- [50] Kumar N, Yu Y-C, Lu YH, Tseng TY (2016) Fabrication of carbon nanotube/cobalt oxide nanocomposites via electrophoretic deposition for supercapacitor electrodes. *J Mater Sci* 51:2320–2329. <https://doi.org/10.1007/s10853-015-9540-9c>
- [51] Dubal DP, Chodankar NR, Caban-Huertas Z, Wolfart F, Vidotti M, Holze R et al (2016) Synthetic approach from polypyrrole nanotubes to nitrogen doped pyrolyzed carbon nanotubes for asymmetric supercapacitors. *J Power Sources* 308:158–165
- [52] Mao H, Shen Y, Zhang Q, Ulaganathan M, Zhao S, Yang Y et al (2016) Highly active and stable heterogeneous catalysts based on the entrapment of noble metal nanoparticles in 3D ordered porous carbon. *Carbon* 96:75–82
- [53] Arrigo R, Schuster ME, Xie Z, Yi Y, Wowsnick G, Sun LL et al (2015) Nature of the N–Pd interaction in nitrogen-doped carbon nanotube catalysts. *ACS Catal* 5:2740–2753
- [54] Dibandjo P, Bois L, Chassagneux F, Cornu D, Letoffe JM, Toury B et al (2005) Synthesis of boron nitride with ordered mesostructure. *Adv Mater* 17:571–574
- [55] Vanyorek L, Meszaros R, Barany S (2014) Surface and electrochemical characterization of surface-oxidized multi-walled N-doped carbon nanotubes. *Colloids Surf A Physicochem Eng Asp* 448:140–146
- [56] Misra A, Tyagi PK, Singh MK, Misra D (2006) FTIR studies of nitrogen doped carbon nanotubes. *Diamond Rel Mater* 15:385–388

- [57] Vinu A, Srinivasu P, Sawant DP, Mori T, Ariga K, Chang J-S et al (2007) Three-dimensional cage type mesoporous CN-based hybrid material with very high surface area and pore volume. *Chem Mater* 19:4367–4372
- [58] Mane GP, Talapaneni SN, Lakhi KS, Ilbeygi H, Ravon U, Al-Bahily K et al (2017) Highly ordered nitrogen-rich mesoporous carbon nitrides and their superior performance for sensing and photocatalytic hydrogen generation. *Angew Chem Int Ed* 56:8481–8485
- [59] Lazar G, Lazar I (2003) IR characterization of a C:H:N films sputtered in Ar/CH<sub>4</sub>/N<sub>2</sub> plasma. *J Non-Cryst Solids* 331:70–78
- [60] Vikkisk M, Kruusenberg I, Ratso S, Joost U, Shulga E, Kink I et al (2015) Enhanced electrocatalytic activity of nitrogen-doped multi-walled carbon nanotubes towards the oxygen reduction reaction in alkaline media. *RSC Adv* 5:59495–59505
- [61] Tan X, Wu X, Hu Z, Ma D, Shi Z (2017) Synthesis and catalytic activity of palladium supported on heteroatom doped single-wall carbon nanohorns. *RSC Adv* 7:29985–29991
- [62] Koós AA, Dowling M, Jurkschat K, Crossley A, Grobert N (2009) Effect of the experimental parameters on the structure of nitrogen-doped carbon nanotubes produced by aerosol chemical vapour deposition. *Carbon* 47:30–37
- [63] Xie K, Xia W, Masa J, Yang F, Weide P, Schuhmann W et al (2016) Promoting effect of nitrogen doping on carbon nanotube-supported RuO<sub>2</sub> applied in the electrocatalytic oxygen evolution reaction. *J Energy Chem* 25:282–288
- [64] Xiao M, Zhu J, Feng L, Liu C, Xing W (2015) Meso/macroporous nitrogen-doped carbon architectures with Iron carbide encapsulated in graphitic layers as an efficient and robust catalyst for the oxygen reduction reaction in both acidic and alkaline solutions. *Adv Mater* 27:2521–2527
- [65] Kotakoski J, Krashennikov A, Ma Y, Foster AS, Nordlund K, Nieminen RM (2005) B and N ion implantation into carbon nanotubes: insight from atomistic simulations. *Phys Rev B* 71:205408
- [66] Sjöström H, Stafström S, Boman M, Sundgren J-E (1995) Superhard and elastic carbon nitride thin films having fullerene-like microstructure. *Phys Rev Lett* 75:1336
- [67] Ewels C, Glerup M (2005) Nitrogen doping in carbon nanotubes. *J Nanosci Nanotechnol* 5:1345–1363
- [68] Chizari K, Sundararaj U (2014) The effects of catalyst on the morphology and physicochemical properties of nitrogen-doped carbon nanotubes. *Mater Lett* 116:289–292
- [69] Sharifi T, Nitze F, Barzegar HR, Tai C-W, Mazurkiewicz M, Malolepszy A et al (2012) Nitrogen doped multi walled carbon nanotubes produced by CVD-correlating XPS and Raman spectroscopy for the study of nitrogen inclusion. *Carbon* 50:3535–3541
- [70] Shan C, Zhao W, Lu XL, O'Brien DJ, Li Y, Cao Z et al (2013) Three-dimensional nitrogen-doped multiwall carbon nanotube sponges with tunable properties. *Nano Lett* 13:5514–5520
- [71] Latorre N, Romeo E, Cazana F, Ubieta T, Royo C, Villacampa J et al (2010) Carbon nanotube growth by catalytic chemical vapor deposition: a phenomenological kinetic model. *J Phys Chem C* 114:4773–4782
- [72] Li R, Zhang P, Huang Y, Zhang P, Zhong H, Chen Q (2012) Pd-Fe<sub>3</sub>O<sub>4</sub>@ C hybrid nanoparticles: preparation, characterization, and their high catalytic activity toward Suzuki coupling reactions. *J Mater Chem* 22:22750–22755
- [73] Chen X, Hou Y, Wang H, Cao Y, He J (2008) Facile deposition of Pd nanoparticles on carbon nanotube microparticles and their catalytic activity for Suzuki coupling reactions. *J Phys Chem C* 112:8172–8176
- [74] Radkevich V, Senko T, Wilson K, Grishenko L, Zaderko A, Diyuk V (2008) The influence of surface functionalization of activated carbon on palladium dispersion and catalytic activity in hydrogen oxidation. *Appl Catal A Gen* 335:241–251
- [75] Chen Y, Wang J, Liu H, Banis MN, Li R, Sun X et al (2011) Nitrogen doping effects on carbon nanotubes and the origin of the enhanced electrocatalytic activity of supported Pt for proton-exchange membrane fuel cells. *J Phys Chem C* 115:3769–3776
- [76] Hachimi A, Merzougui B, Hakeem A, Laoui T, Swain GM, Chang Q et al (2015) Synthesis of nitrogen-doped carbon nanotubes using injection-vertical chemical vapor deposition: effects of synthesis parameters on the nitrogen content. *J Nanomater* 16:425
- [77] Morjan I, Morjan I, Ilie A, Scarisoreanu M, Gavrila L, Dumitrache F et al (2017) The study of nitrogen inclusion in carbon nanotubes obtained by catalytic laser-induced chemical vapour deposition (C-LCVD). *Appl Surf Sci* 425:440–447
- [78] Hsiao C-H, Lin J-H (2017) Growth of a superhydrophobic multi-walled carbon nanotube forest on quartz using flow-vapor-deposited copper catalysts. *Carbon* 124:637–641
- [79] Bulusheva L, Okotrub A, Fedoseeva YV, Kurennya A, Asanov I, Vilkov O et al (2015) Controlling pyridinic, pyrrolic, graphitic, and molecular nitrogen in multi-wall carbon nanotubes using precursors with different N/C ratios in aerosol assisted chemical vapor deposition. *Phys Chem Chem Phys* 17:23741–23747
- [80] Sing KS, Williams RT (2004) Physisorption hysteresis loops and the characterization of nanoporous materials. *Adsorpt Sci Technol* 22:773–782

- [81] ALOthman ZA (2012) A review: fundamental aspects of silicate mesoporous materials. *Mater* 5:2874–2902
- [82] Du J, Zhao R, Jiao G (2013) The short-channel function of hollow carbon nanoparticles as support in the dehydrogenation of cyclohexane. *Int J Hydrogen Energy* 38:5789–5795
- [83] Zhao Y, Li C-H, Yu Z-X, Yao K-F, Ji S-F, Liang J (2007) Effect of microstructures of Pt catalysts supported on carbon nanotubes (CNTs) and activated carbon (AC) for nitrobenzene hydrogenation. *Mater Chem Phys* 103:225–229
- [84] Tangestaninejad S, Moghadam M, Mirkhani V, Mohamadpoor-Baltork I, Ghani K (2009) Alkene epoxidation catalyzed by molybdenum supported on functionalized MCM-41 containing N–S chelating Schiff base ligand. *Catal Commun* 10:853–858
- [85] Kotal M, Bhowmick AK (2013) Multifunctional hybrid materials based on carbon nanotube chemically bonded to reduced graphene oxide. *J Phys Chem C* 117:25865–25875
- [86] Huang H, Leung DY (2011) Complete oxidation of formaldehyde at room temperature using TiO<sub>2</sub> supported metallic Pd nanoparticles. *ACS Catal* 1:348–354
- [87] H-q Song, Zhu Q, X-j Zheng, X-g Chen (2015) One-step synthesis of three-dimensional graphene/multiwalled carbon nanotubes/Pd composite hydrogels: an efficient recyclable catalyst for Suzuki coupling reactions. *J Mater Chem A* 3:10368–10377
- [88] Xu Y, Wang T, He Z, Zhong A, Huang K (2016) Carboxyl-containing microporous organic nanotube networks as a platform for Pd catalysts. *RSC Adv* 6:39933–39939
- [89] Artok L, Bulut H (2004) Heterogeneous Suzuki reactions catalyzed by Pd (0)–Y zeolite. *Tetrahedron Lett* 45:3881–3884
- [90] Pourkhosravani M, Dehghanpour S, Farzaneh F (2016) Palladium nanoparticles supported on zirconium metal organic framework as an efficient heterogeneous catalyst for the Suzuki–Miyaura coupling reaction. *Catal Lett* 6:499–508
- [91] Primo A, Liebel M, Fo Quignard (2009) Palladium coordination biopolymer: a versatile access to highly porous dispersed catalyst for Suzuki reaction. *Chem Mater* 21:621–627
- [92] Arrigo R, Wrabetz S, Schuster ME, Wang D, Villa A, Rosenthal D et al (2012) Tailoring the morphology of Pd nanoparticles on CNTs by nitrogen and oxygen functionalization. *Phys Chem Chem Phys* 14:10523–10532
- [93] Deraedt C, Astruc D (2013) “Homeopathic” palladium nanoparticle catalysis of cross carbon–carbon coupling reactions. *Acc Chem Res* 47:494–503
- [94] Corma A, Garcia H, Leyva A (2005) Catalytic activity of palladium supported on single wall carbon nanotubes compared to palladium supported on activated carbon: study of the Heck and Suzuki couplings, aerobic alcohol oxidation and selective hydrogenation. *J Mol Catal A: Chem* 230:97–105
- [95] Alonso-Morales N, Ruiz-Garcia C, Palomar J, Heras F, Calvo L, Rodriguez JJ et al (2017) Hollow nitrogen-or boron-doped carbon submicrospheres with a porous shell: preparation and application as supports for hydrodechlorination catalysts. *Ind Eng Chem Res* 56:7665–7674
- [96] Bidabehere CM, Garcia JR, Sedran U (2017) Transient effectiveness factor in porous catalyst particles. Application to kinetic studies with batch reactors. *Chem Eng Res Des* 118:41–50
- [97] Dong Y, Wu X, Chen X, Wei Y (2017) N-Methylimidazole functionalized carboxymethylcellulose-supported Pd catalyst and its applications in Suzuki cross-coupling reaction. *Carbohydr Polym* 160:106–114
- [98] Dong W, Zhang L, Wang C, Feng C, Shang N, Gao S et al (2016) Palladium nanoparticles embedded in metal–organic framework derived porous carbon: synthesis and application for efficient Suzuki–Miyaura coupling reactions. *RSC Adv* 6:37118–37123
- [99] Kwon TH, Cho KY, Baek K-Y, Yoon HG, Kim BM (2017) Recyclable palladium–graphene nanocomposite catalysts containing ionic polymers: efficient Suzuki coupling reactions. *RSC Adv* 7:11684–11690
- [100] Veisi H, Azadbakht R, Saeidifar F, Abdi MR (2017) Schiff base-functionalized multi walled carbon nano tubes to immobilization of palladium nanoparticles as heterogeneous and recyclable nanocatalyst for Suzuki reaction in aqueous media under mild conditions. *Catal Lett* 147:976–986
- [101] Hajjighorbani M, Hekmati M (2016) Pd nanoparticles deposited on isoniazid grafted multi walled carbon nanotubes: synthesis, characterization and application for Suzuki reaction in aqueous media. *RSC Adv* 6:88916–88924
- [102] Zhang A, Liu M, Liu M, Xiao Y, Li Z, Chen J et al (2014) Homogeneous Pd nanoparticles produced in direct reactions: green synthesis, formation mechanism and catalysis properties. *J Mater Chem A* 2:1369–1374
- [103] Yu L, Han Z (2016) Palladium nanoparticles on polyaniline (Pd@ PANI): a practical catalyst for Suzuki cross-couplings. *Mater Lett* 184:312–314
- [104] Ji R, Zhai S-R, Meng Y-Y, Xiao Z-Y, An Q-D (2017) Deposition of N-doped carbon layers inside acidic ZrSBA-15: significant enhancement of catalytic performance of Pd

- NPs toward benzyl alcohol aerobic oxidation. *J Sol-Gel Sci Technol* 84:180–191
- [105] Li Y, Huang J, Hu X, Lam FL-Y, Wang W, Luque R (2016) Heterogeneous Pd catalyst for mild solventfree oxidation of benzyl alcohol. *J Mol Catal A: Chem* 425:61–67
- [106] Hao Y, Wang S, Sun Q, Shi L, Lu A-H (2015) Uniformly dispersed Pd nanoparticles on nitrogen-doped carbon nanospheres for aerobic benzyl alcohol oxidation. *Chin J Catal* 36:612–619
- [107] Dimitratos N, Villa A, Wang D, Porta F, Su D, Prati L (2006) Pd and Pt catalysts modified by alloying with Au in the selective oxidation of alcohols. *J Catal* 244:113–121
- [108] Marco Y, Roldán L, Armenise S, García-Bordejé E (2013) Support-induced oxidation state of catalytic Ru nanoparticles on carbon nanofibers that were doped with heteroatoms (O, N) for the decomposition of NH<sub>3</sub>. *ChemCatChem* 5:3829–3834
- [109] Puthiaraj P, Pitchumani K (2014) Palladium nanoparticles supported on triazine functionalised mesoporous covalent organic polymers as efficient catalysts for Mizoroki–Heck cross coupling reaction. *Green Chem* 16:4223–4233
- [110] Chang F, Guo J, Wu G, Liu L, Zhang M, He T et al (2015) Covalent triazine-based framework as an efficient catalyst support for ammonia decomposition. *RSC Adv* 5:3605–3610
- [111] Bell TE, Zhan G, Wu K, Zeng HC, Torrente-Murciano L (2017) Modification of ammonia decomposition activity of ruthenium nanoparticles by N-doping of CNT supports. *Top Catal* 60:1251–1259
- [112] Tessonnier J-P, Rosenthal D, Hansen TW, Hess C, Schuster ME, Blume R et al (2009) Analysis of the structure and chemical properties of some commercial carbon nanostructures. *Carbon* 47:1779–1798
- [113] Hao Y, Qingwen L, Jin Z, Zhongfan L (2003) The effect of hydrogen on the formation of nitrogen-doped carbon nanotubes via catalytic pyrolysis of acetonitrile. *Chem Phys Lett* 380:347–351
- [114] Wang J, Huang R, Feng Z, Liu H, Su D (2016) Multi-walled carbon nanotubes as a catalyst for gas-phase oxidation of ethanol to acetaldehyde. *Chemosuschem* 9:1820–1826
- [115] Abdullahi I, Davis TJ, Yun DM, Herrera JE (2014) Partial oxidation of ethanol to acetaldehyde over surface-modified single-walled carbon nanotubes. *Appl Catal A Gen* 469:8–17
- [116] Shinde VM, Skupien E, Makkee M (2015) Synthesis of highly dispersed Pd nanoparticles supported on multi-walled carbon nanotubes and their excellent catalytic performance for oxidation of benzyl alcohol. *Catal Sci Technol* 5:4144–4153
- [117] Wilson D, Langell M (2014) XPS analysis of oleylamine/oleic acid capped Fe<sub>3</sub>O<sub>4</sub> nanoparticles as a function of temperature. *Appl Surf Sci* 303:6–13